



ORIGINAL ARTICLE

Impact of design parameters and stress-strain diagrams on the ultimate limit state of instability in reinforced concrete columns

Impacto dos parâmetros de dimensionamento e do diagrama tensão-deformação no estado limite último de instabilidade em pilares de concreto armado

Nicolle Lorrayne Domingos Guerra^a Ricardo Carrazedo^a ^aUniversidade de São Paulo – USP, Escola de Engenharia de São Carlos – EESC, Departamento de Engenharia de Estruturas, São Carlos, SP, Brasil

Received 22 February 2024

Revised 29 May 2024

Accepted 19 June 2024

Abstract: In high-rise buildings, high-strength concrete (HSC) columns are often used to reduce cross-sectional dimensions while supporting high loads. However, this design decision may result in structures that are more susceptible to deformation, raising concerns about their structural stability. Therefore, this paper aims to study the key design parameters such as concrete strength, column slenderness, eccentricity, longitudinal reinforcement ratio, and creep effects that may lead the columns to the ultimate limit state of instability. Besides, this work studies the use of various stress-strain diagrams to represent the concrete behavior according to standards and codes. Consequently, it was noted that columns with a lower ratio of eccentricity to the effective length, higher slenderness, and lower longitudinal reinforcement are more prone to reaching the ultimate limit state of instability. The use of different stress-strain diagrams had a marginal impact on determining the ultimate limit state, but accounting for the creep effect was essential for accurate results. Assessing the ultimate bearing capacity using various stress-strain diagrams yielded different outcomes, highlighting the significance of choosing one in accordance with safety standards. The new stress-strain diagram proposed by Brazilian code decreased the ultimate load capacity of most analyzed columns and reduced the number of columns experiencing failure due to instability.

Keywords: column, instability, slenderness, reinforced concrete, stress-strain diagram, NBR 6118:2023.

Resumo: Em edifícios altos, pilares de concreto de alta resistência (HSC) são frequentemente usados para reduzir as dimensões da seção transversal enquanto suportam cargas elevadas. No entanto, essa decisão pode resultar em estruturas mais suscetíveis à deformação, o que pode resultar em problemas relacionados à estabilidade estrutural. Portanto, este trabalho visa estudar os principais parâmetros, resistência do concreto, esbeltez, excentricidade, taxa de armadura longitudinal e efeitos de fluência, que podem levar os pilares ao estado limite último de instabilidade. Além disso, este trabalho estuda o uso de vários diagramas tensão-deformação para representar o comportamento do concreto de acordo com as normas. Consequentemente, observou-se que colunas com uma menor razão entre excentricidade e comprimento efetivo, maior esbeltez e menor taxa armadura longitudinal são mais propensas a atingir o estado limite último de instabilidade. O uso de diferentes diagramas tensão-deformação tem pequeno impacto na determinação do estado limite último, mas considerar o efeito de fluência é essencial. Avaliar a capacidade de carga última usando diferentes diagramas tensão-deformação resultou em resultados diferentes, destacando a importância de escolher um de acordo com as normas de projeto. O novo diagrama tensão-deformação proposto pelo código brasileiro diminuiu a capacidade de carga última da maioria das colunas analisadas e reduziu a quantidade de pilares atingindo a falha por instabilidade.

Palavras-chave: pilares, instabilidade, esbeltez, concreto de alta resistência, diagrama tensão-deformação, NBR 6118:2023.

How to cite: N. L. D. Guerra and R. Carrazedo, "Impact of design parameters and stress-strain diagrams on the ultimate limit state of instability in reinforced concrete columns," *Rev. IBRACON Estrut. Mater.*, vol. 17, no. 2, e17216, 2024, <https://doi.org/10.1590/S1983-41952024000200016>

Corresponding author: Nicolle Lorrayne Domingos Guerra. E-mail: n.guerra@usp.br

Financial support: This study was financed in part by the Coordenação de Aperfeiçoamento de Pessoal de Nível Superior – Brasil (CAPES) – Finance Code 001.

Conflict of interest: Nothing to declare.

Data Availability: The information required to reproduce the findings of this study is reported in the paper. Other data such as computer codes will be made available by the corresponding author upon reasonable request.



This is an Open Access article distributed under the terms of the Creative Commons Attribution License, which permits unrestricted use, distribution, and reproduction in any medium, provided the original work is properly cited.

1 INTRODUCTION

High-strength concrete (HSC) columns are extensively employed in high-rise buildings when the objective is to reduce cross-sectional dimensions while accommodating high applied loads. Nonetheless, this design choice can inadvertently lead to structures that are more susceptible to deformation, thereby potentially giving rise to concerns regarding structural stability. Consequently, the ultimate load-bearing capacity of HSC columns can be governed by instability, a contrast to normal-strength concrete (NSC) columns where the governing factor is usually the strength.

The issue of deformation in columns when using high-strength concrete becomes evident when comparing its strength value with Young's modulus. As concrete strength increases, Young's modulus does not increase proportionally, meaning the stiffness of the column does not progress at an equivalent rate. Consequently, under substantial loads and significant deflection, internal forces within the column increase, leading the column to withstand higher moments, which is commonly referred to as second-order effects.

The contribution of second-order effects significantly impacts the ultimate load-bearing capacity of columns, which represents the maximum load they can support without failure. As a result, this influence can heighten the column's susceptibility to the ultimate limit state of instability rather than to material failure. Therefore, various parameters influence the behavior of columns, impacting their bearing capacity and vulnerability to the ultimate limit state of instability. In addition to concrete strength, other crucial factors include column slenderness, first-order eccentricity relative to the effective length of the column, longitudinal reinforcement ratio, and the effects of concrete creep.

Experimental studies have been conducted to understand the behavior of columns under eccentric loads. It was noticed that the load-carrying capacity of columns decreases with an increase in both slenderness and first-order eccentricity [1]–[3], and this behavior is further pronounced in high-strength concrete columns [4]. Additionally, smaller values of first-order eccentricity result in columns that are more susceptible to the ultimate limit state of instability, due to a greater amplification of second-order effects compared to first-order effects, a phenomenon that is especially evident in slender columns [5] and is magnified in high-strength concrete columns [6].

Furthermore, columns featuring a higher longitudinal reinforcement ratio provide enhanced stability, a characteristic of particular significance in the case of slender columns. This effect becomes more pronounced with a simultaneous increase in concrete strength, thereby accenting the effectiveness of rising longitudinal reinforcement in high-strength slender columns [6]. As such, there is a noticeable elevation in the load-carrying capacity of columns exhibiting a substantial longitudinal reinforcement ratio [6]–[8].

Another factor that must be considered in column analysis is the effect of creep, which tends to reduce the load-carrying capacity attributed to amplified deflection resulting from deformation, which is particularly evident in the context of slender columns [9]. Furthermore, Lahoud [10] reported that the load-bearing capacity of high-strength concrete columns is notably influenced by the creep coefficient.

The standards aim to address these influences on column forces and mitigate the risk of reaching the ultimate limit state of instability by incorporating second-order effects through amplifying bending moments. Nevertheless, it remains crucial to examine these influences in order to fully grasp the circumstances that drive a column towards the ultimate limit state of instability. In instances where a column displays this risk, simply increasing the longitudinal reinforcement ratio to enhance cross-sectional strength may not yield the desired effect and can potentially result in column failure.

Thus, it is possible to correlate the load-bearing capacity of a column with its tendency towards either stability or material failure. This is accomplished using the axial force-bending moment interaction diagrams (N-M), a method introduced by MacGregor et al. [9] and later applied by Pallarés et al. [5], Kim and Yang [6], Marí and Helleland [11], Germain and Espion [12], and Fenollosa et al. [13]. The column interaction diagrams help to determine the ultimate limit state that a column reaches under its ultimate load, by comparing it to the ultimate combination of N-M forces that the section can withstand (failure surface).

Hence, this study aims to identify the occurrence of the ultimate limit state of instability, considering various crucial parameters in column design, and evaluating their influence on the ultimate load-bearing capacity of columns. These parameters include concrete strength, column slenderness, the ratio of eccentricity to the effective length, longitudinal reinforcement ratio, and the impact of creep. The study will also provide recommendations regarding the most suitable stress-strain diagram for accurately representing concrete behavior and defining the ultimate limit state of a column. The investigation focuses on square, pin-ended columns subjected to axial loading with a first-order eccentricity along one axis, resulting in uniaxial bending.

2 M-N INTERACTION DIAGRAMS

Column interaction diagrams are employed to determine the ultimate limit state of a column when it reaches its ultimate load. The methodology introduced by MacGregor et al. [9] receives significant endorsement from authors for studying slender columns and offers a straightforward practical application in cases of uniaxial bending, as indicated by Germain and Espion [12]. Consequently, given the focus of this research on pin-ended columns, it aligns with the type of columns examined here.

Considering the effect of uniaxial bending, the constant first-order moment along the column's height adds to the maximum second-order moment occurring at the mid-height of the column due to deflections resulting from geometric nonlinearity. This is exemplified by Figure 1. Column 1 is identified as short, column 2 has moderate slenderness and column 3 is identified as slender. As a result, the critical section emerges at the mid-height of the column, where the axial force-bending moment interaction of the column can be compared with the axial force-bending moment interaction resisted by the cross-section (failure surface).

Consequently, it facilitates the identification of two possible types of column failure: material failure and stability failure. Column 1 (Figure 1), characterized by minimal deflection, is identified as a short column, exhibiting material failure when the load-bearing capacity is reached. In scenarios where the column remains stable under deflection Δ_2 , but the ultimate axial load and bending moment at the mid-height section may surpass the strength of that specific cross-section, material failure arises. This is exemplified by column 2 (Figure 1). On the other hand, if the peak load is reached before encountering the failure surface, as observed when subjected to deflection Δ_3 , stability failure occurs. This is exemplified by column 3 (Figure 1).

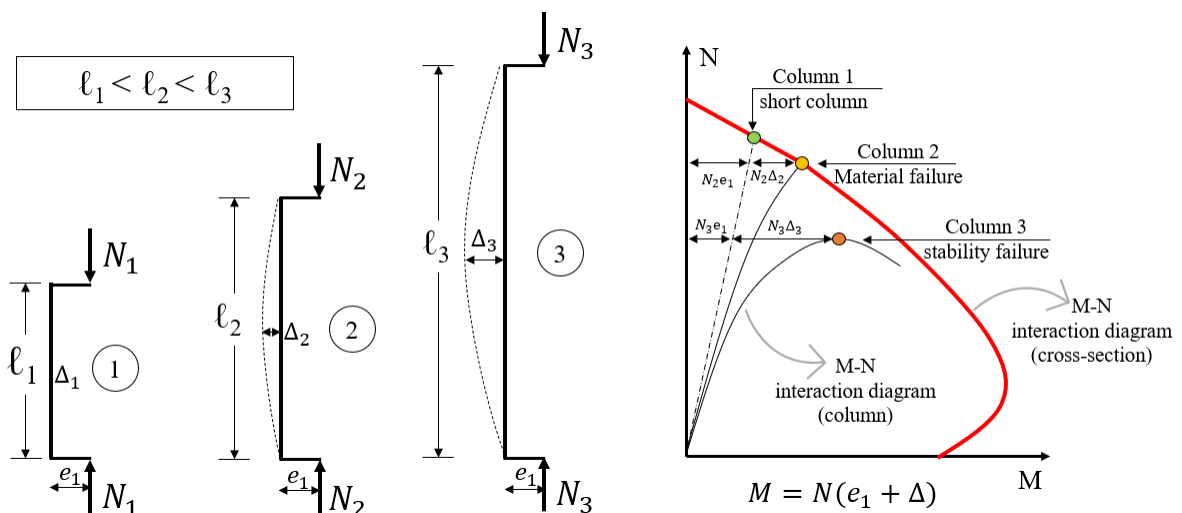


Figure 1. Load and moment in slender column.

In order to understand the concept of material or instability failure, it is essential to recognize that concrete columns exhibit non-linear material behavior and are subjected to eccentric loads. These conditions result in a configuration where equilibrium becomes unachievable past the limit point. As a result, the system cannot support forces that go beyond the set limit. Thus, when the peak load is achieved even if the cross-section has the capacity to withstand it, the ultimate load is determined by the ultimate limit state of instability.

To determine the ultimate limit state of the column as material failure or instability using the M-N interaction diagram method, it is necessary to establish the axial load-bending moment relationship resisted by the column's cross-section, as well as the axial load-bending moment relationship that the column is subjected to.

2.1 Axial load-bending moment interaction resisted by the column's cross-section

To establish the axial load-bending moment interaction resisted by the column's cross-section, the corresponding resistant bending moment (M_{Rd}) needs to be identified for each resistant axial force (N_{Rd}), which is equal to the applied

force (N_{sd}). This procedure allows for the determination of the resistance envelope (failure surface) according to the provisions of ABNT NBR 6118:2023 [14] that establish the material's ultimate limit state.

To achieve this, it is necessary to determine the strain distribution along the depth of a rectangular cross-section. This is possible due to strain compatibility, which dictates that plane sections remain plane and that steel strain matches concrete strain at all points. Consequently, this provides the stress distribution through the material's stress-strain diagram, resulting in the bending moment resisted by the section. This process allows for the determination of the axial load-bending moment interaction resisted by the column's cross-section, which forms the resistance envelope.

2.2 Axial load-bending moment interaction of the column

The axial force-bending moment interaction of the column is easily determined when using geometric and material linearity, as it is the result of the multiplication between the load and its eccentricity, corresponding to the first-order theory. However, it is necessary to consider the second-order effects and the material behavior, which lead to nonlinearity between the applied load and the resulting moment.

Therefore, to determine the applied load-moment interaction it is necessary to implement those conditions to represent the column behavior. To that, it is possible to do a numerical simulation using the Abaqus® software, which considers the material and geometric nonlinearity of the column, as it employs finite element analysis and offers various models to represent the steel and the concrete. To define a simulation model that provided satisfactory data on the column's behavior, aiming for the shortest pre-processing and processing time, it was used Guerra and Carrazedo [15] research.

The authors have verified two distinct two-dimensional models on finite element Abaqus® software to obtain a load-deflection diagram. They have suggested the use of the model which adopts a beam element (B23 element type) with a discrete rebar embedded into the concrete section using Abaqus/Standard, according to Figure 2, with the Cast Iron Plasticity as a simplified representation of the concrete.

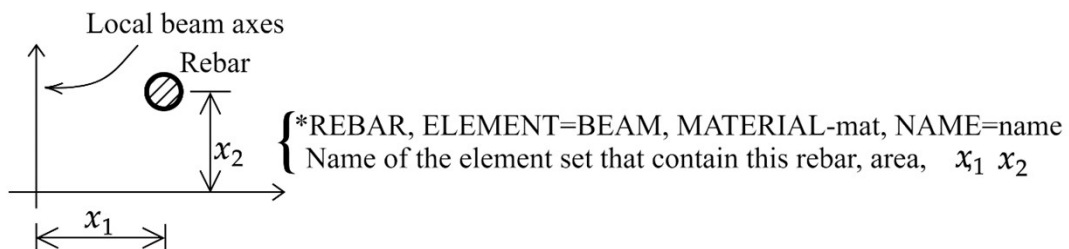


Figure 2. Rebar in beam Elements.

This paper utilized Abaqus® software to analyze the axial load-bending moment interaction of the column. According to ABNT NBR 6118:2023 [14], the peak stress of concrete should be taken as 1.1 times the design compressive strength (f_{cd}) to ensure proper representation of structural deformability. Therefore, stress-strain diagrams that include the concrete brittleness coefficient were not adopted to describe the column interaction diagram; they were retained only to define the columns' cross-section interaction diagram. Additionally, it is important to note the inclusion of a sharp stress drop upon reaching the ultimate strain, illustrating material failure in both concrete and steel on the stress-strain diagram.

3 STRESS-STRAIN DIAGRAMS

Normal-strength concrete exhibits nonlinearity right from the start of loading, leading to a gradual loss of stiffness as cracking advances. However, as the concrete strength class increases, porosity decreases, and there is an enhancement in the transition zone, demanding higher stress levels for the initiation of cracks. The result of this behavior is the abrupt rupture of the concrete, which is characterized as brittle, and a stress-strain diagram that closely approximates linearity.

In the interest of simplifying the development of the stress-strain diagram, which is typically acquired through axial compression tests on specimens, several authors have put forth empirically derived expressions. An example is Carreira and Chu's [16] expression that effectively describes the stress-strain diagram's behavior.

Thereby, the stress-strain behavior of concrete under compression varies across different codes and standards. Consequently, it is essential to determine the most appropriate diagram for each specific scenario to ensure an accurate representation of concrete behavior. This paper, therefore, explores the utilization of various stress-strain diagrams.

The stress-strain diagram recommended by ABNT NBR 6118:2014 [17] (Figure 3a) boasts a well-established history of usage in Brazilian standards and carries the endorsement of EN 1992-1-1:2004 [18] for structural design, using the Equation 1. Values of the peak load and the ultimate load are presented ahead according to each analysis, and the value of n is presented in Equations 2 or 3.

$$\sigma_c = 0,85 f_{cd} \left[1 - \left(1 - \frac{\varepsilon_c}{\varepsilon_{c2}} \right)^n \right] \quad (1)$$

$$n = 2 \quad (f_{ck} \leq 50 \text{ MPa}) \quad (2)$$

$$n = 1,4 + 23 \cdot \left[\frac{90 - f_{ck}}{100} \right]^4 \quad (f_{ck} > 50 \text{ MPa}) \quad (3)$$

The revision of the code in ABNT NBR 6118:2023 [14] (Figure 3b) introduced a reduction in the peak stress on the diagram to account for concrete's brittleness (η_c), as shown in Equation 4. The value of η_c can be adopted according to Equation 5 or 6. This modification was adapted from the stress-strain diagram proposed by Moccia et al. [19], which maintained the strain at the peak stress and ultimate strain as consistent for both normal-strength concrete and high-strength concrete, besides of maintaining a value of n equal to 2. This stress-strain diagram has been incorporated into section 8.1.2 of EN 1991-1-1:2023 [20] (Figure 3c).

It is crucial to emphasize that the application of uniform strain limits ($\varepsilon_{c2} = 2.0\%$ and $\varepsilon_{cu} = 3.5\%$) across all concrete strengths does not adequately capture concrete behavior, as deformations are influenced by the concrete's strength class.

$$\sigma_c = 0,85 \eta_c f_{cd} \left[1 - \left(1 - \frac{\varepsilon_c}{\varepsilon_{c2}} \right)^n \right] \quad (4)$$

$$\eta_c = 1 \quad (f_{ck} \leq 40 \text{ MPa}) \quad (5)$$

$$\eta_c = \left(\frac{40}{f_{ck}} \right)^{1/3} \quad (f_{ck} > 40 \text{ MPa}) \quad (6)$$

Furthermore, EN 1992-1-1:2004 [18] (Figure 3d) suggests a diagram for nonlinear structural analyses, which is permissible under the Brazilian code with adaptations, according to Equations 7, 8 and 9. Lastly, an additional noteworthy diagram is the adaptation of the ABNT NBR 6118:2014 [17] diagram, incorporating deformations that consider concrete creep, as proposed by Fusco [21] (Figure 3e).

$$\frac{\sigma_c}{f_{cm}} = \frac{k\eta - \eta^2}{1 + (k-2)\eta} \quad (7)$$

$$\eta = \frac{\varepsilon_c}{\varepsilon_{c1}} \quad (8)$$

$$k = 1,05 E_{cm} \cdot \frac{|\varepsilon_{c1}|}{f_{cm}} \quad (9)$$

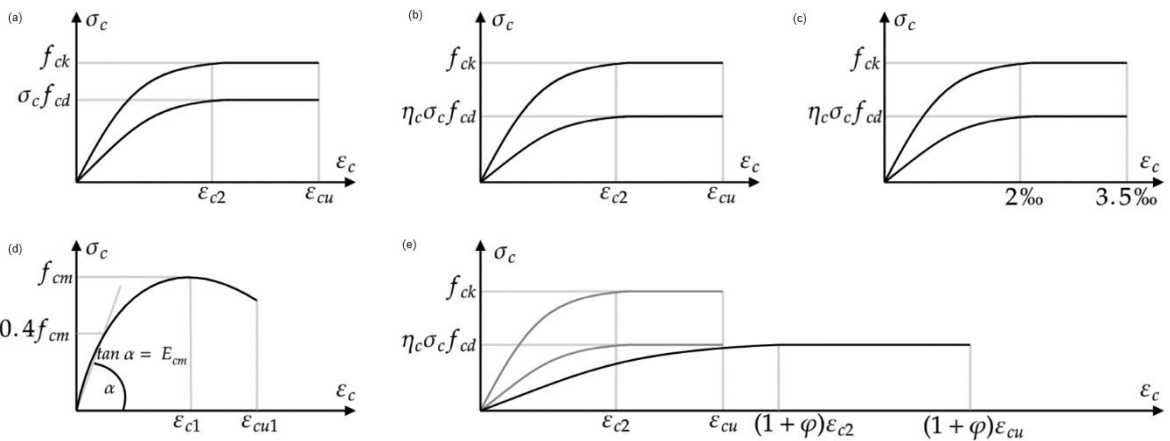


Figure 3. Stress-strain diagrams: (a) ABNT NBR 6118:2014, (b) EN 1992-1-1:2004, (c) ABNT NBR 6118:2023, (d) EN 1992-1-1:2023, and (e) ABNT NBR 6118:2014 adapted to consider concrete creep.

The stress-strain diagram is utilized to depict the behavior of concrete in both the axial load-bending moment interaction of the column and of the column's cross-section. As previously mentioned, the determination of the resistance envelope in this study adheres to the guidelines outlined in ABNT NBR 6118:2023 [14]. Therefore, only the parabola-rectangle stress-strain diagram was utilized.

Additionally, in describing the column's interaction, it is crucial to consider that the peak stress of concrete should be 1.1 times the design compressive strength (f_{cd}) to accurately represent structural deformability, as indicated in ABNT NBR 6118:2023 [14]. Consequently, concrete's brittleness coefficient (η_c), should not be used.

Nevertheless, the stress-strain diagram adopted for steel represents its behavior using the elastic perfectly plastic model, a widely recognized approach, included in ABNT NBR 6118:2023 [14]. The yield strength, considering characteristic values, was set at 500 MPa, resulting in a design value of 435 MPa. The Young's modulus adopted was 210 GPa, with an ultimate strain of 10%.

4 PARAMETRIC STUDY

The square column subjected to uniaxial bending has a side length of 20 cm and symmetrical reinforcement, with the rebar center located 3 cm from each side.

The concrete strength was evaluated using both normal-strength concrete (C40) and high-strength concrete (C80). The column slenderness values in the parametric study ranged from the lower limit ($\lambda=35$) to the upper limit ($\lambda=200$) specified by ABNT NBR 6118:2023 [14]. This range encompasses significant values such as $\lambda=90$, from which the calculation of second-order effects is required, demanding more complex methods and the consideration of creep, and $\lambda=140$, which requires the general method. Additionally, intermediate values were selected at $\lambda=60$ and $\lambda=115$.

In assessing the eccentricity parameter, the ratio of eccentricity to the effective length of the column (e/l_e) was employed. To represent column imperfections, values of $e/l_e = 0.001$, $e/l_e = 0.004$, $e/l_e = 0.016$, and $e/l_e = 0.048$ were utilized to analyze the behavior of the column under varied eccentricities.

For the longitudinal reinforcement, some reinforcement ratios were considered: the minimum ($\rho=0.4\%$) and maximum ($\rho=4\%$) ratios, as well as intermediate values commonly used in actual design ($\rho=1\%$ and $\rho=2\%$). Considering the importance of the creep effect, particularly since ABNT NBR 6118:2023 [14] requires its consideration for slenderness ratios of $\lambda=90$ and above, the columns were assessed under two conditions: without creep ($\phi = 0$) and with creep ($\phi = 2$).

Analyses on the columns were conducted using the stress-strain diagrams illustrated in Figure 3. For normal-strength concrete columns, the axial load-bending moment interaction was defined using stress-strain diagrams from ABNT NBR 6118:2014 [17] (C40-NBR14), EN 1992-1-1:2004 [18] (C40-EUR04), and an adaptation of ABNT NBR 6118:2014 [17] to account for the creep effect according to Fusco [21] (C40-NBR14-F2). Diagrams from Figure 3a, Figure 3d, and Figure 3e, with a peak stress of $1.1 f_{cd}$, were employed respectively. The resistance envelope for these analyses was determined utilizing the parabola-rectangle stress-strain diagram from Figure 3a.

For high-strength concrete columns, a similar methodology was applied. The stress-strain diagrams from ABNT NBR 6118:2014 [17] (C80-NBR14), EN 1992-1-1:2004 [18] (C80-EUR04), and the adaptation by Fusco [21] considering the creep effect (C80-NBR14-F2) were utilized. The respective diagrams were Figure 3a, Figure 3d, and Figure 3e, again with a peak stress of $1.1 f_{cd}$, and the resistance envelope was likewise determined using the parabolarectangle stress-strain diagram from Figure 3a.

Furthermore, stress-strain diagrams from ABNT NBR 6118:2023 [14] (C80-NBR23) and EN 1992-1-1:2023 [20] (C80-EUR23) were incorporated into the analyses. However, these diagrams from Figure 3b and Figure 3c, respectively, were employed to determine the axial load-bending moment interaction of the cross-section, as the η_c coefficient should only be applied to describe the resistance envelope. Consequently, the axial load-bending moment interaction for these columns was determined using diagrams from ABNT NBR 6118:2014 [17] (Figure 3a) and EN 1992-1-1:2004 [18] (Figure 3d), both with a peak stress of $1.1 f_{cd}$.

By using all those diagrams, this led to 8 analyses of the columns. In each analysis, variations were made to the slenderness index, the ratio of eccentricity to the effective length of the column, and the longitudinal reinforcement ratios. This resulted in a total of 96 different columns for each analysis.

As a result, there are 768 columns with varying characteristics, each producing an axial load-bending moment diagram for the column, as displayed in Table 1. To compare this data with the axial load-bending moment diagram of the cross-section and to determine the ultimate limit state of all the columns, as the strength of the column's cross-section was not determined using the same stress-strain diagram when analyzing its deformed shape, information from Table 2 was employed.

Table 1. Properties of the axial load-bending moment of the columns

Stage	Strength classes	ϕ	Stress-strain diagrams	Peak stress	ϵ_{c1}	ϵ_{cu1}	ϵ_{c2}	ϵ_{cu}	E	λ	e/l_e	ρ
C40-NBR14	C40	0	Figure 3a	$1.1 f_{cd}$	–	–	2.000	3.500	31875 MPa	35	0.001	1%
C40-EUR04			Figure 3d	$1.1 f_{cd}$	2.000	3.500	–	–				
C40-NBR14-F2		2	Figure 3e	$1.1 f_{cd}$	–	–	6.000	10.500				
C80-NBR14	C80	0	Figure 3a	$1.1 f_{cd}$	–	–	2.516	2.604	45132 MPa	90	0.004	2%
C80-EUR04			Figure 3d	$1.1 f_{cd}$	2.800	2.803	–	–		115	0.016	3%
C80-NBR23		Figure 3a	$1.1 f_{cd}$	–	–	2.516	2.604	140	0.048	4%		
C80-EUR23		Figure 3d	$1.1 f_{cd}$	2.800	2.803	–	–	200				
C80-NBR14-F2		2	Figure 3e	$1.1 f_{cd}$	–	–	7.548	7.812				

Table 2. Properties of the axial load-bending moment of the cross-section

Stage	Strength classes	ϕ	Stress-strain diagrams	Peak stress	ϵ_{c2}	ϵ_{cu}	E	ρ
C40-NBR14	C40	0	Figure 3a	$0.85 f_{cd}$	2.000	3.500	31875 MPa	1%
C40-EUR04			Figure 3a					
C40-NBR14-F2		2	Figure 3a					
C80-NBR14	C80	0	Figure 3a	$0.85 f_{cd}$	2.516	2.604	45132 MPa	2%
C80-EUR04			Figure 3a					
C80-NBR23		Figure 3b	$0.85 \eta_c f_{cd}$	2.516	2.604	4%		
C80-EUR23		Figure 3c	$0.85 \eta_c f_{cd}$	2.000	3.500			
C80-NBR14-F2		2	Figure 3a	$0.85 f_{cd}$	2.516	2.604		

5 RESULTS AND DISCUSSIONS

After defining the axial load-bending moment of all 768 columns, the columns interaction method was applied to define their ultimate limit state, which could be of instability or material failure. Moreover, it was possible to define the ultimate load of the columns, which possibilities to understand their bearing capacity of according to different parameters.

5.1 Ultimate limit state

The analysis resulted in 768 columns with varying characteristics, each one producing an axial load-bending moment diagram for the column. As described before, each column was compared with the cross-section resistance envelope, which would determine the ultimate limit state of all the columns.

Figure 4 illustrates axial load-bending moment diagrams for six distinct columns. These columns are characterized by normal-strength concrete, the absence of creep effects, and adherence to the stress-strain diagram specified in ABNT NBR 6118:2014 [17] (C40-NBR14). Furthermore, these columns exhibit minimal levels of eccentricity and longitudinal reinforcement, with e/ℓ_e at 0.001 and ρ at 0.4%. Thus, the image represents columns under these specific conditions, with slenderness (λ) indices ranging from 35 to 200.

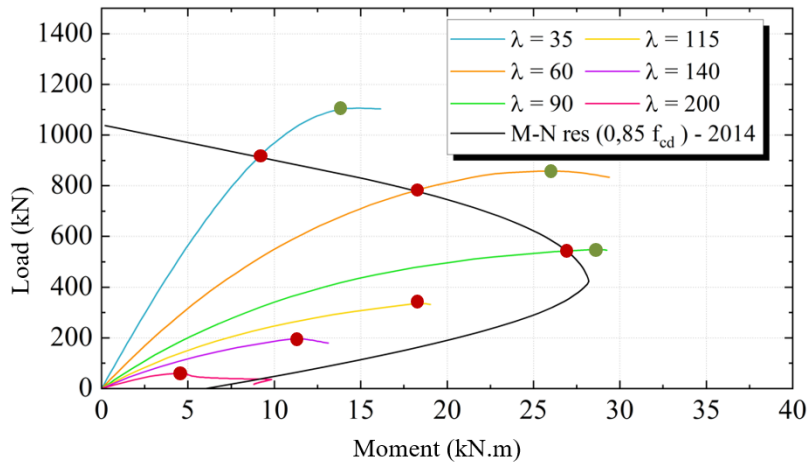


Figure 4. Interaction diagram of the columns with normal-strength concrete (C40), e/ℓ_e at 0.001, ρ at 0.4%, absence of creep effects and slenderness (λ) varying from 35 to 200.

The columns with the green data points that extend beyond the resistance envelope have reached the ultimate limit state of material failure. This occurs when the cross-section fails before the column loses its stability. Thus, the ultimate load would be represented by the red data points. Conversely, the columns with the red data points within the resistance envelope have reached the ultimate limit state of instability. In this case, instability occurs even though the cross-section could endure the forces.

Another noteworthy observation from Figure 4 is that utilizing distinct stress-strain diagrams to construct axial load-bending moment diagrams for both column and cross-section led to the occurrence of the maximum load outside the boundaries of the resistance envelope when the ultimate limit state is material failure. However, when the same stress-strain diagram or peak load is employed, the maximum load tends to align precisely with the resistance envelope. This alignment can create challenges in distinguishing between the ultimate limit state of material failure and that of instability.

Continuing with this analysis, it becomes feasible to ascertain the ultimate limit state for all 768 columns. Table 3 illustrates all 288 columns with normal-strength concrete and Table 4 illustrates all 480 columns with high-strength concrete. This comprehensive analysis brings into focus the impacts of concrete strength, the influence of creep effects, eccentricity, slenderness, reinforcement, and the selection of the stress-strain diagram. Additionally, it provides an avenue to assess the effectiveness of the M-N interaction diagram method.

In all stages, it became evident that columns with a smaller ratio of eccentricity to the effective length and higher slenderness tend to approach the ultimate limit state of instability. The presence of a small first-order effect due to a minimal eccentricity magnifies the significance of any second-order effect. As slenderness increases, second-order effects become more pronounced, leading to intensified column deflection. Consequently, columns in this condition tend to experience instability before reaching the point of material failure.

It is also noteworthy that an increase in the longitudinal reinforcement ratio reduces the tendency toward the ultimate limit state of instability, effectively generating more stable columns. Therefore, it is important to highlight cases with a high longitudinal reinforcement ratio, where the column exhibits minimal eccentricity and a high slenderness index, and yet, it reaches the ultimate limit state of material failure.

Table 3. Ultimate limit states of normal-strength concrete columns

Stage	$e/t_e \rightarrow$	0.001				0.004				0.016				0.048			
	ρ (%) \rightarrow	0.4	1.0	2.0	4.0	0.4	1.0	2.0	4.0	0.4	1.0	2.0	4.0	0.4	1.0	2.0	4.0
C40-NBR14	$\lambda = 35$																
	$\lambda = 60$																
	$\lambda = 90$																
	$\lambda = 115$																
	$\lambda = 140$																
	$\lambda = 200$																
C40-EUR04	$\lambda = 35$																
	$\lambda = 60$																
	$\lambda = 90$																
	$\lambda = 115$																
	$\lambda = 140$																
	$\lambda = 200$																
C40-NBR14-F2	$\lambda = 35$																
	$\lambda = 60$																
	$\lambda = 90$																
	$\lambda = 115$																
	$\lambda = 140$																
	$\lambda = 200$																
		Ultimate Limit State of instability															
		Ultimate Limit State of material failure															

Table 4. Ultimate limit states of high-strength concrete columns

Stage	$e/t \rightarrow$	0.001				0.004				0.016				0.048			
	ρ (%) \rightarrow	0.4	1.0	2.0	4.0	0.4	1.0	2.0	4.0	0.4	1.0	2.0	4.0	0.4	1.0	2.0	4.0
C80-NBR14	$\lambda = 35$																
	$\lambda = 60$																
	$\lambda = 90$																
	$\lambda = 115$																
	$\lambda = 140$																
	$\lambda = 200$																
C80-EUR04	$\lambda = 35$																
	$\lambda = 60$																
	$\lambda = 90$																
	$\lambda = 115$																
	$\lambda = 140$																
	$\lambda = 200$																
C80-NBR23	$\lambda = 35$																
	$\lambda = 60$																
	$\lambda = 90$																
	$\lambda = 115$																
	$\lambda = 140$																
	$\lambda = 200$																
C80-EUR23	$\lambda = 35$																
	$\lambda = 60$																
	$\lambda = 90$																
	$\lambda = 115$																
	$\lambda = 140$																
	$\lambda = 200$																
C80-NBR14-F2	$\lambda = 35$																
	$\lambda = 60$																
	$\lambda = 90$																
	$\lambda = 115$																
	$\lambda = 140$																
	$\lambda = 200$																
		Ultimate Limit State of instability															
		Ultimate Limit State of material failure															

In such cases, the high longitudinal reinforcement ratio allows for significant deformations, substantially increasing second-order effects. This, in turn, drives the cross-section to reach its maximum strength, even though the column remains stable under increasing applied loads. Consequently, it is possible to notice columns with significant second order effects failing due to material when they have a high longitudinal reinforcement ratio, slenderness, and minimal eccentricity.

When using the ABNT NBR 6118:2014 [17] stress-strain diagram, increasing the concrete strength resulted in a shift from the ultimate limit state of material failure to instability for two columns with identical parameters. These columns shared characteristics such as an e/ℓ_e ratio of 0.004, a λ value of 90, and longitudinal reinforcement ratios (ρ) of 0.4% and 1%. Notably, their peak loads approached balanced failure, occurring when concrete reaches its maximum compression stress and steel reaches its maximum tensile stress simultaneously, typically at the boundary between domains 3 and 4, resulting in maximum moment.

When peak load is in proximity to this condition, even slight changes can significantly impact the results by using M-N interaction diagram method. Therefore, although increasing concrete strength did lead to more columns reaching the ultimate limit state of instability, the effect was not particularly pronounced.

The behavior of columns as their peak loads approach balanced failure also elucidates the instability observed in C40-NB14 analysis of the column with an e/ℓ_e ratio of 0.004, a slenderness ratio (λ) of 60, and a longitudinal reinforcement ratio (ρ) of 0.4%. Despite having parameters that typically do not predispose it to instability, Table 3 identifies instability upon application of the ultimate load.

An essential factor influencing the ultimate limit state of instability is the consideration of the creep effect. This factor played a significant role in the failure due to instability. The introduction of the creep effect resulted in increased column deformations, even in moderately slender columns, leading to a higher tendency to instability. This phenomenon is notably prominent in normal-strength concrete columns, which previously exhibited a lower predisposition towards instability. It is important to emphasize that the creep effect analysis considers only a single value of creep coefficient.

Going beyond these parameters, an examination of various stress-strain diagrams prescribed by different codes sheds light on their distinct influences. When comparing EN 1992-1-1:2004 [18] with ABNT NBR 6118:2014 [17], disparities emerge only in specific instances (e/ℓ_e equal to 0.004 and λ equal to 90), and these differences were observed in normal-strength concrete.

An important comparison arises when contrasting the analyses of C80-NBR23 and C80-EUR23 with C80-NBR14. This comparison highlights the influence of stress-strain diagrams that include the concrete brittleness coefficient in determining the resistance envelope and the ultimate limit state of the concrete. To illustrate this, a comparison of the three axial load-bending moment interactions of the column cross-sections is presented in Figure 5.

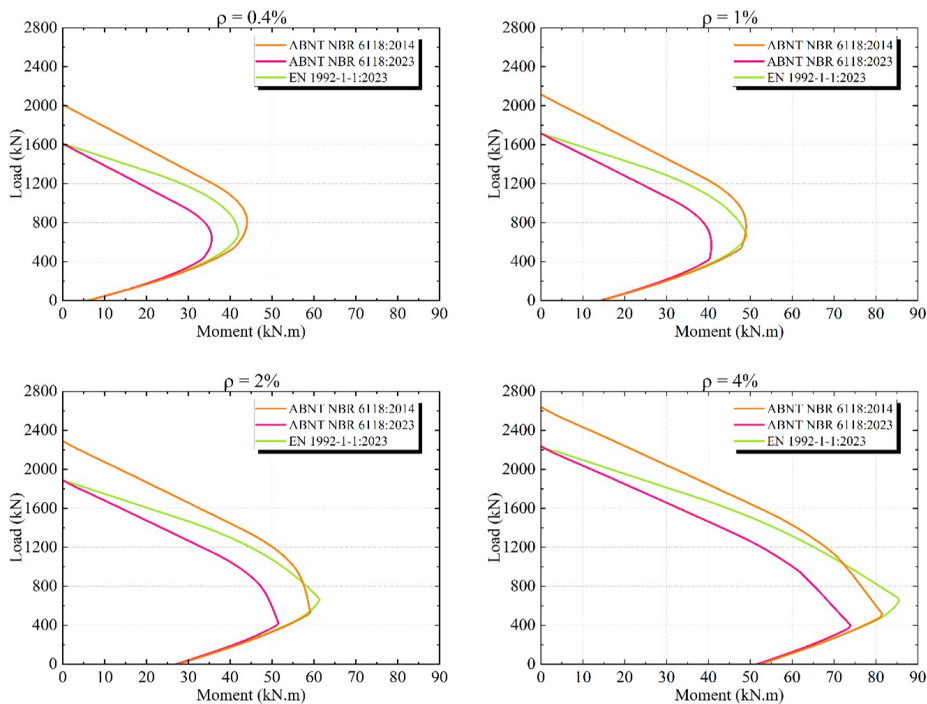


Figure 5. Comparison of the resistance envelope: ABNT NBR 6118:2014 [17], ABNT NBR 6118:2023 [14], and EN 1992-1-1:2023 [20]

It is noted that for the same load, the resistance envelope determined by the ABNT NBR 6118:2014 [17] stress-strain diagram presents the highest moment compared to those determined by ABNT NBR 6118:2023 [14] and EN 1992-1-1:2023 [20], while the ABNT NBR 6118:2023 [14] stress-strain diagram presents the smallest moment. Therefore, it is evident that C80-NBR14 columns have the highest probability of instability failure, while C80-NBR23 columns have the lowest probability.

This is clearly observed as some C80-NBR23 columns exhibit material failure with a slenderness index of 115, whereas C80-EUR23 columns show instability. Furthermore, with C80-NBR14, columns with an e/ℓ_c ratio equal to 0.004 and ρ of 0.4% or 1% reach the ultimate limit state of instability at a slenderness index of 90, while those columns experience material failure when using both other stress-strain diagrams.

5.2 Ultimate load

The ultimate load, which the column can reach before attaining the ultimate limit states, is defined differently depending on the type of failure. In the case of instability, it is defined by the peak load (maximum load), while for material failure, it is determined by the load that crosses the resistance failure surface. Consequently, this allows for an examination of each parameter's impact on the column's ultimate load and how the selection of the stress-strain diagram can influence its value.

Considering that neither the stress-strain diagram from ABNT NBR 6118:2014 [17] nor the EN 1992-1-1:2004 [18] stress-strain for cross-section design incorporates the use of the brittleness factor, Figure 6 displays the ultimate load values for normal and high-strength concrete when employing the stress-strain diagram from ABNT NBR 6118:2014 [17] (C40-NBR14), serving as a reference value for the other results.

As expected, increasing the column's slenderness reduces the ultimate load. This reduction is accentuated when the eccentricity ratio increases. Conversely, the ultimate load increases with a higher rate of longitudinal reinforcement.

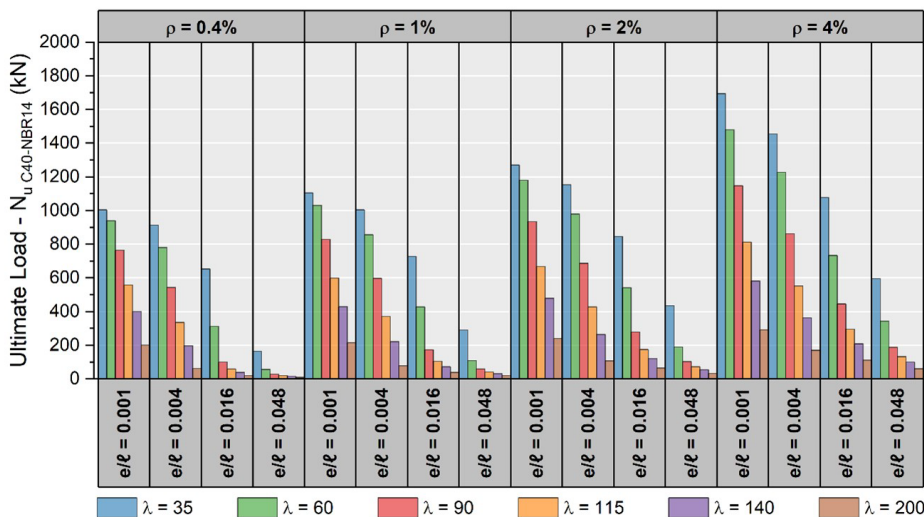


Figure 6. Ultimate load on columns (C40-NBR14).

When comparing the ultimate load as concrete transitions from normal-strength to high-strength, Figure 7 reveals that it does not significantly increase the load for certain columns. Those that experience instability achieve their ultimate load at the point of peak load, making the enhancement of cross-section strength less crucial in raising the ultimate load.

Furthermore, for columns primarily failing due to bending moments, the increase in concrete strength has a less significant impact, attributed to the type of failure. Consequently, the enhancement in concrete strength becomes vital in boosting the ultimate load only when column failure primarily results from compression, and this scenario applies to shorter columns.

The ultimate load of columns using the stress-strain diagram from ABNT NBR 6118:2014 [17] was compared to other stress-strain relationships. To normal-strength concrete, Figure 8 shows that, especially for columns that failed due to instability, there is a significant reduction in the ultimate load when using the EN 1992-1-1:2004 [18] stress-strain diagram. Additionally, the consideration of the creep effect results in a substantial reduction in the ultimate load, particularly for slender columns with smaller eccentricity, as displayed in Figure 9.

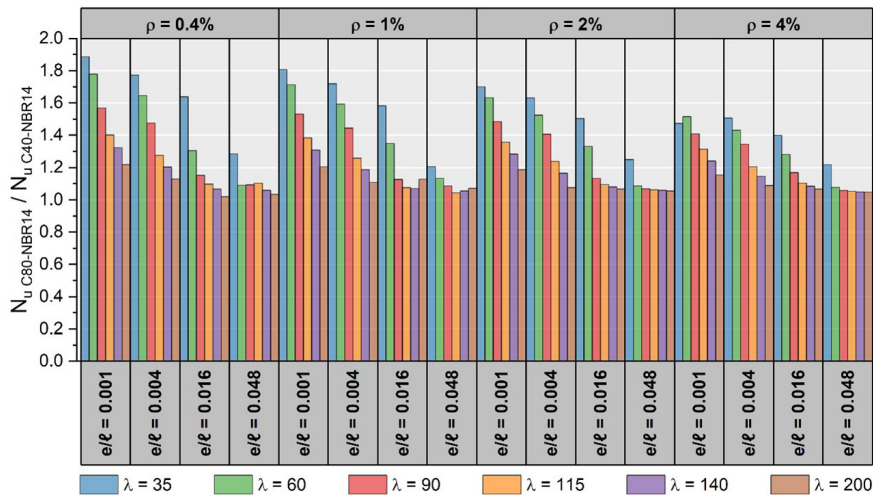


Figure 7. Ratio between the ultimate load of high-strength (C80-NBR14) concrete and normal-strength concrete (C40-NBR14).

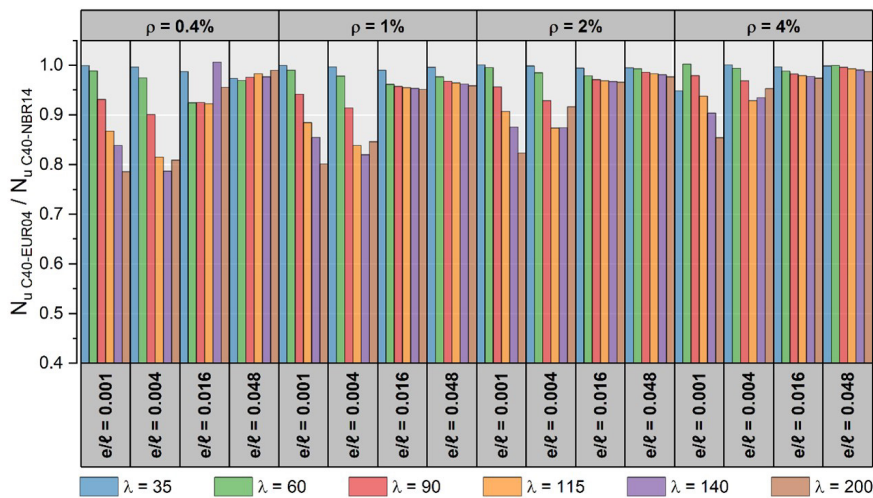


Figure 8. Ratio between the ultimate load of normal-strength concrete with EN 1992-1-1:2004 (C40-EUR04) and ABNT NBR 6118:2014 (C40-NBR14) stress-strain diagrams.

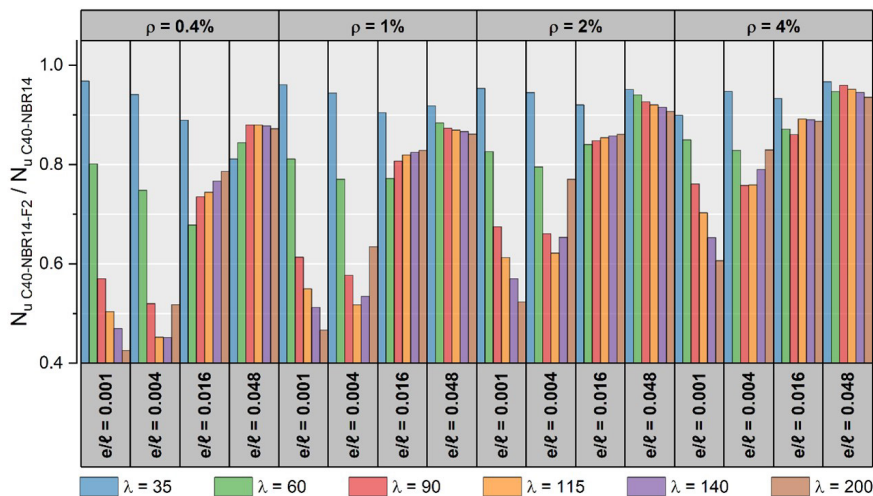


Figure 9. Ratio between the ultimate load of normal-strength concrete with ABNT NBR 6118:2014 considering creep effect (C40-NBR14-F2) and ABNT NBR 6118:2014 (C40-NBR14) stress-strain diagrams.

The impact of different stress-strain diagrams from ABNT NBR 6118:2014 [17] on the ultimate load of high-strength concrete columns is examined in Figure 10. Initially, the increase in concrete strength reduces the influence of using the EN 1992-1-1:2004 [18] stress-strain diagram.

Upon comparing the ultimate load using the stress-strain diagram from ABNT NBR 6118:2023 [14], it becomes evident that the ultimate load primarily decreases for columns with lower eccentricity. This is because concrete plays a significant role in compression-related column failure, especially in shorter columns, as shown in Figure 11. When using the EN 1992-1-1:2023 [20] stress-strain diagram (Figure 12), a similar behavior is observed; however, the reduction in ultimate load is less pronounced. Additionally, the consideration of creep effects (Figure 13) has a more significant impact on high-strength concrete, substantially reducing the ultimate load.

Upon analysis, it becomes evident that the choice of the stress-strain diagram can significantly impact the determined ultimate load-bearing capacity of the column. The EN 1992-1-1:2004 [18] stress-strain diagram primarily affects normal-strength concrete columns. The reduction in ultimate load predominantly affects columns that are susceptible to instability failure, which is crucial for preventing such failures. On the other hand, high-strength concrete columns may be influenced by different diagrams.

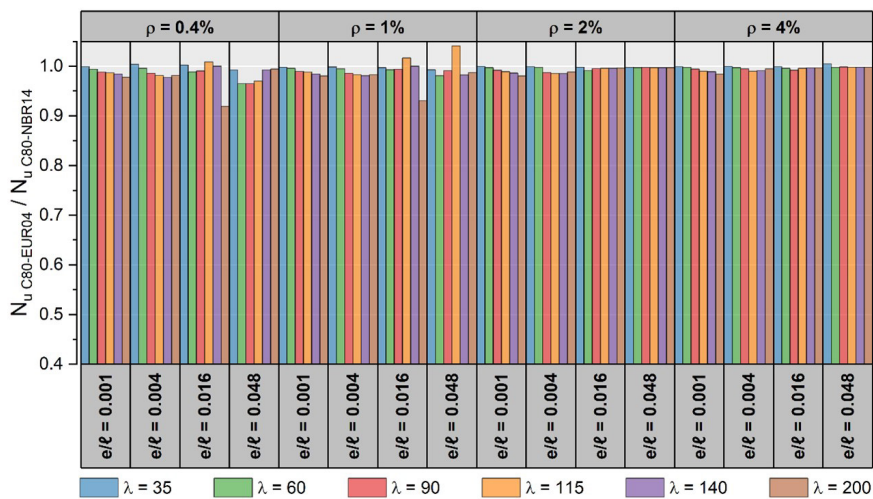


Figure 10. Ratio between the ultimate load of high-strength concrete with EN 1992-1-1:2004 (C80-EUR04) and ABNT NBR 6118:2014 (C80-NBR14) stress-strain diagrams.

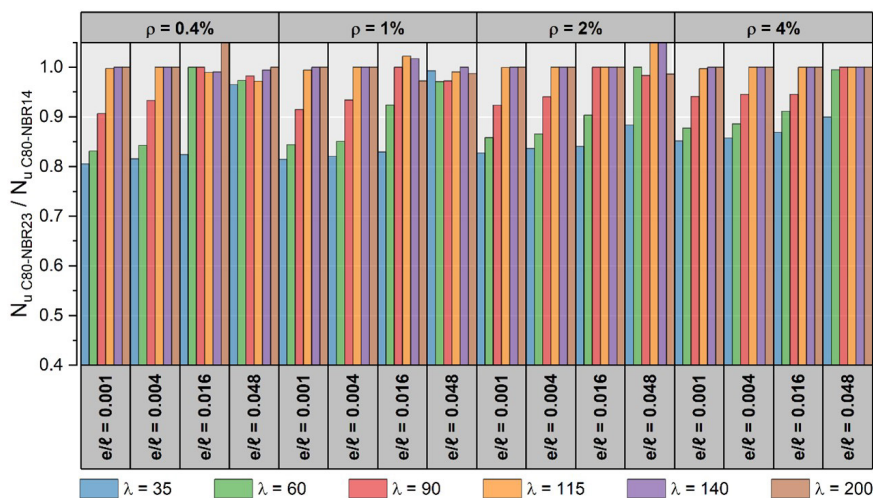


Figure 11. Ratio between the ultimate load of high-strength concrete with ABNT NBR 6118:2023 (C80-NBR23) and ABNT NBR 6118:2014 (C80-NBR14) stress-strain diagrams.

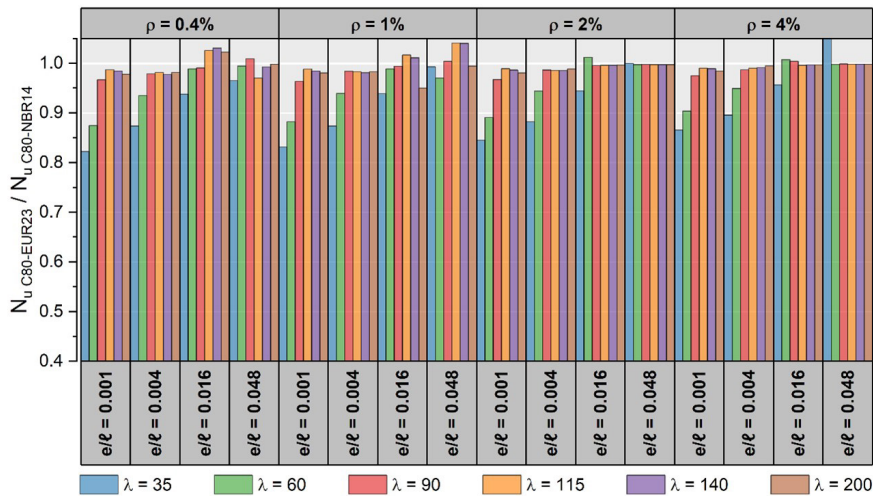


Figure 12. Ratio between the ultimate load of high-strength concrete with EN 1992-1-1:2023 (C80-EUR23) and ABNT NBR 6118:2014 (C80-NBR14) stress-strain diagrams.

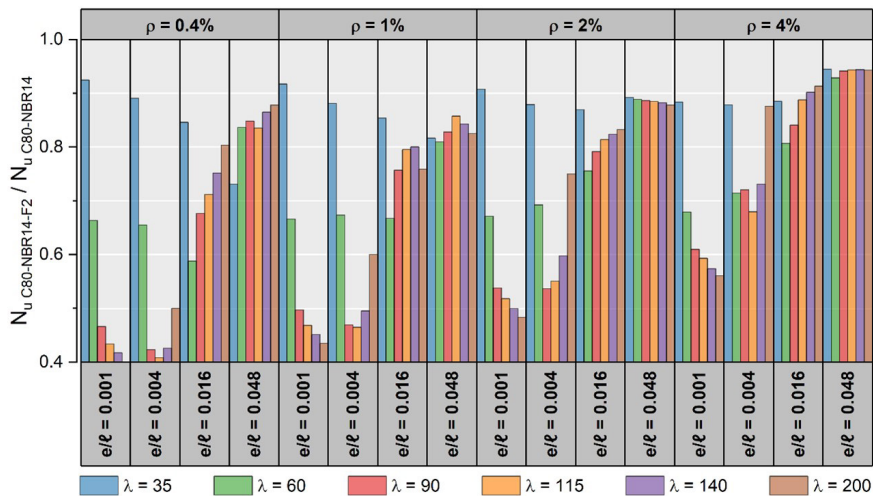


Figure 13. Ratio between the ultimate load of high-strength concrete with ABNT NBR 6118:2023 considering creep effect (C80-NBR14-F2) and ABNT NBR 6118:2014 (C80-NBR14) stress-strain diagrams.

The new Brazilian code, ABNT NBR 6118:2023 [14], reduces the ultimate load capacity primarily in shorter columns, and this effect is more pronounced when the load is applied with lower eccentricity due to the brittleness factor. When using the stress-strain diagram from EN 1992-1-1:2023 [20], the ultimate loads are slightly higher than those obtained with the ABNT NBR 6118:2023 [14] stress-strain diagram, in accordance with the resistance envelope presented in Figure 5.

Moreover, even though creep effect analysis considers only a single value of creep coefficient, it is notable the significance of its consideration. It reduces the ultimate load-bearing capacity of the columns, especially in slender columns with lower eccentricity. This effect becomes even more pronounced in columns with high-strength concrete.

6 CONCLUSIONS

This paper identified the occurrence of the ultimate limit state of instability in columns, considering various parameters crucial in column design. The M-N interaction diagrams method, which used stability analysis with finite element to define the column’s load path, was revealed to be effective in this context. It is important to note that when applying the stress-strain diagram to determine the axial load-bending moment of the column, a factor of 1.1 should be used to determine

concrete strength, whereas for the axial load-bending moment of the cross-section (representing the resistance envelope), a factor equal to 0.85 is recommended, and in the case of brittle concrete, it includes the coefficient η_c .

Additionally, it was observed that columns with a smaller ratio of eccentricity to the effective length and higher slenderness are more susceptible to reaching the ultimate limit state of instability. On the other hand, an increase in the longitudinal reinforcement ratio reduces the tendency of reaching the ultimate limit state of instability. Therefore, it is worth noting that some columns experienced material failure with minimal eccentricity and high slenderness, especially when the longitudinal reinforcement ratio was higher, even though they exhibited significant second-order effects. Moreover, although increasing concrete strength did lead to more columns reaching the ultimate limit state of instability, the effect was not particularly pronounced.

Choosing to use the stress-strain diagram from ABNT NBR 6118:2023 [14] to represent the resistance envelope results in more columns reaching the ultimate limit state of material failure. Besides, considering the creep effect proved to be a significant factor in determining the ultimate limit state, even though its analysis considers only a single value of creep coefficient. Some columns even failed due to instability at a slenderness index of 60, demonstrating that they did not need to be particularly slender to experience instability failure.

When analyzing the ultimate bearing capacity of the columns, it was observed that an increase in column slenderness resulted in a reduction of the ultimate load, which became more pronounced with higher eccentricity ratios. Conversely, an increased rate of longitudinal reinforcement led to higher ultimate loads. However, it is noteworthy that enhancing concrete strength did not proportionally increase the ultimate load. Rather, the enhancement in the ultimate load was particularly notable in cases of material failure.

In examining stress-strain diagrams used for interaction diagrams, it became evident that the diagram from EN 1992-1-1:2004 [18] had a more substantial impact on normal-strength concrete columns, leading to a reduction in their load-bearing capacity, especially for columns prone to instability, an outcome crucial to preventing such failures. Additionally, the implementation of the new Brazilian code, ABNT NBR 6118:2023 [14], along with the stress-strain diagram by EN 1992-1-1:2023 [20], revealed that the reduction in ultimate load capacity was most significant in shorter columns, owing to the brittleness factor particularly affecting them. As previously observed, slender columns have a higher tendency to fail due to instability. Therefore, the reduction in ultimate load occurring mostly in short columns does not effectively prevent such failures.

ACKNOWLEDGEMENTS

The authors gratefully acknowledge CAPES (Coordenação de Aperfeiçoamento de Pessoal de Nível Superior, Brazil) doctorate scholarship and financial support provided. Valuable comments by the anonymous reviewers are also cheerfully acknowledged.

REFERENCES

- [1] A. B. Dantas, "Estudo de pilares de concreto armado submetidos à flexão composta reta," M.S. thesis, Univ. Brasília, Brasília, DF, 2006.
- [2] C. E. L. Melo, "Análise experimental e numérica de pilares birrotulados de concreto armado submetidos a flexo-compressão normal," Ph.D. dissertation, Univ. Brasília, Brasília, DF, 2009.
- [3] G. S. Santos, "Análise experimental e numérica de pilares de concreto armado submetido a flexão composta reta," M.S. thesis, Univ. Brasília, Brasília, DF, 2009.
- [4] C. Claeson and K. Gylltoft, "Slender high-strength concrete subjected to eccentric loading," *J. Struct. Eng.*, vol. 124, no. 3, pp. 233–240, 1998, [http://doi.org/10.1061/\(ASCE\)0733-9445\(1998\)124:3\(233\)](http://doi.org/10.1061/(ASCE)0733-9445(1998)124:3(233)).
- [5] L. Pallarés, J. L. Bonet, P. F. Miguel, and M. A. Fernández Prada, "Experimental research on high strength concrete slender columns subjected to compression and biaxial bending forces," *Eng. Struct.*, vol. 30, no. 7, pp. 1879–1894, 2008, <http://doi.org/10.1016/j.engstruct.2007.12.005>.
- [6] J. K. Kim and J. K. Yang, "Buckling behaviour of slender high-strength concrete columns," *Eng. Struct.*, vol. 17, no. 1, pp. 39–51, Nov 1995, [http://doi.org/10.1016/0141-0296\(95\)91039-4](http://doi.org/10.1016/0141-0296(95)91039-4).
- [7] L. Leite, J. L. Bonet, L. Pallarés, P. F. Miguel, and M. A. Fernández-Prada, "Experimental research on high strength concrete slender columns subjected to compression and uniaxial bending with unequal eccentricities at the ends," *Eng. Struct.*, vol. 48, pp. 220–232, 2013, <http://doi.org/10.1016/j.engstruct.2012.07.039>.
- [8] H. A. Kottb, N. F. El-Shafey, and A. A. Torkey, "Behavior of high strength concrete columns under eccentric loads," *HBRC J.*, vol. 11, no. 1, pp. 22–34, 2015, <http://doi.org/10.1016/j.hbrj.2014.02.006>.

- [9] J. G. MacGregor, J. E. Breen, and E. O. Pfrang, "Design of slender concrete columns," *J. Am. Concr. Inst.*, vol. 67, no. 1, pp. 6–28, Jan 1970, <http://doi.org/10.14359/7254>.
- [10] A. E. Lahoud, "Slenderness effects in high-strength concrete columns," *Can. J. Civ. Eng.*, vol. 18, no. 5, pp. 765–771, Feb 1991, <http://doi.org/10.1139/191-093>.
- [11] A. R. Mari and J. Hellesland, "Lower slenderness limits for rectangular reinforced concrete columns," *J. Struct. Eng.*, vol. 131, no. 1, pp. 86–95, Jan 2005, [http://doi.org/10.1061/\(ASCE\)0733-9445\(2005\)131:1\(85\)](http://doi.org/10.1061/(ASCE)0733-9445(2005)131:1(85)).
- [12] O. Germain and B. Espion, "Slender high-strength RC columns under eccentric compression," *Mag. Concr. Res.*, vol. 57, no. 6, pp. 361–370, Aug 2005, <http://doi.org/10.1680/macrc.2005.57.6.361>.
- [13] E. Fenollosa, I. Cabrera, V. Llopis, and A. Alonso, "Non-linear analysis of slender high strength concrete column," *Civ. Eng. J.*, vol. 5, no. 7, pp. 1440–1451, 2019, <http://doi.org/10.28991/cej-2019-03091343>.
- [14] Associação Brasileira de Normas Técnicas, *Projeto de Estruturas de Concreto*, ABNT NBR 6118, 2023.
- [15] N. L. D. Guerra and R. Carrazedo, "Numerical model of high-strength reinforced concrete columns subjected to the ultimate limit state of instability," in *CILAMCE*, Foz do Iguaçu, 2022, pp. 1–7.
- [16] D. J. Carreira and K. Chu, "Stress-strain relationship for reinforced concrete in compression," *J. Am. Concr. Inst.*, vol. 83, no. 1, pp. 21–28, 1986, <http://doi.org/10.14359/1756>.
- [17] Associação Brasileira de Normas Técnicas, *Projeto de Estruturas de Concreto - Procedimento*, ABNT NBR 6118, 2014.
- [18] European Committee for Standardization, *EUROCODE 2 – Design of Concrete Structures – Part 1-1: General Rules and Rules for Buildings*, EN 1992-1-1:2004, 2004.
- [19] F. Moccia, Q. Yu, M. F. Ruiz, and A. Muttoni, "Concrete compressive strength: from material characterization to a structural value," *Eng. Struct.*, vol. 30, no. 7, pp. 1879–1894, 2008.
- [20] European Committee for Standardization, *EUROCODE 2 – Design of Concrete Structures – Part 1-1: General Rules and Rules for Buildings, Bridges and Civil Engineering Structures*, EN 1992-1-1:2023, 2023. [In approval].
- [21] P. B. Fusco, *Estruturas de Concreto: Solicitações Normais*, 1a ed. Rio de Janeiro, Brazil: Guanabara Dois S.A., 1981.

Author contributions: NLDG: conceptualization, bibliographic research, methodology, data analysis, writing, revising; RC: conceptualization, supervision, revising, formal analysis.

Editors: Mauro Real, Daniel Carlos Taissum Cardoso.